Iranian Journal of Basic Medical Sciences
ijbms.mums.ac.ir

Development of a hybrid micelle–hydrogel system for topical delivery of doxorubicin to skin cancer cells

Majid Zia-Behbahani [1, 2], Elahehnaz Parhizkar [1], Mahdokht Hossein Aghdaie [3], Elaheh Esfandiari [3], Shohreh Alipour [4*], Fatemeh Ahmadi [1*]

[1] Department of Pharmaceutics, School of Pharmacy, Shiraz University of Medical Sciences, Shiraz, Iran
[2] Students Research Committee, Shiraz University of Medical Sciences, Shiraz, Iran
[3] Transplant Research Center, Shiraz University of Medical Sciences, Shiraz, Iran
[4] Department of Quality Control, School of Pharmacy, Shiraz University of Medical Sciences, Shiraz, Iran

ARTICLE INFO

Article type:
Original

Article history:
Received: Dec 27, 2025
Accepted: May 18, 2026

Keywords:
Doxorubicin
Hyaluronic acid
Hydrogel
Polymeric micelle
Skin cancer

ABSTRACT

Objective(s): Topical delivery of anti-neoplastic agents could circumvent many drawbacks of chemotherapy in skin cancer. This study aims to develop a hybrid Hyaluronic acid-oleic acid (HA-C18) micelle–alginate hydrogel as a topical system for doxorubicin (DOX), enhancing skin penetration, providing controlled release, and localized therapy for skin cancer.

Materials and Methods: DOX-loaded micelles (DOX-PMs) were prepared from the synthesized amphiphilic substance (HA-C18) and incorporated into an alginate hydrogel. Micelles were characterized for size, drug loading, and *in vitro* release behavior. pH and viscosity of the hydrogel were also evaluated. *Ex vivo* permeation through rat skin was investigated for DOX solution, DOX in hydrogel, and DOX-PMs-hydrogel. Finally, cytotoxicity activity and flow cytometry analysis were also performed on the B16F10 cell line.

Results: Size and drug loading of micelles were about 221.4±27 nm and 4.32±0.4%, respectively. pH values, and viscosity of hydrogel were 4.51±0.02, and 3.2 Pa.s, respectively. DOX was released in a burst and sustained manner after 72 h. Results showed that micelles markedly enhanced DOX permeation, achieving a 2.1-fold increase over free drug and a 9.2-fold increase over hydrogel. DOX micelles exhibited lower cytotoxic activity against B16F10 cells compared to free DOX, due to the slower release from the micelles. Finally, in both quantitative and qualitative flow cytometry analyses, the cellular uptake was evident, and the uptake rate was lower than that of free DOX.

Conclusion: The findings indicate that a hybrid micelle–hydrogel platform enables controlled delivery of DOX, enhancing topical efficacy in skin cancer while minimizing systemic exposure in a patient-compatible manner.

▶ Please cite this article as:
Zia-Behbahani M, Parhizkar E, Aghdaie MH, Esfandiari E, Alipour Sh, Ahmadi F. Development of a hybrid micelle–hydrogel system for topical delivery of doxorubicin to skin cancer cells. Iran J Basic Med Sci 2026; 29:

Introduction

In recent years, skin cancer has emerged as one of the malignancies with a significant increase in incidence. Generally, skin cancer is categorized into two main types: melanoma and non-melanoma skin cancer (NMSC). Melanoma arises from pigment-producing cells known as melanocytes (1). Melanoma is the most common malignancy, especially among Caucasian populations, and its incidence has been increasing worldwide. However, the mortality rate associated with melanoma has remained stable or has slightly decreased (2). Despite recent advances, melanoma remains challenging to treat (3). The prognosis for metastatic melanoma is particularly poor due to its aggressive nature and resistance to treatment. Although melanoma represents only approximately 1% of all malignant skin neoplasms, it remains the most aggressive and lethal form of skin cancer (2, 4-11).

Early detection of skin cancer is crucial for successful treatment (12). Over the past few years, several treatment methods have been approved by the U.S. Food and Drug Administration (FDA), including surgery, chemotherapy (e.g., dacarbazine), radiotherapy, photodynamic therapy (PDT), immunotherapy, or targeted therapy (4).

Overall, there are two primary limitations in skin cancer treatment: First, side effects that can lead to skin and gastrointestinal toxicity, typically associated with immune reactions (13-15). Second, decreased treatment efficacy, which can result from resistance to immunotherapy, chemotherapy, targeted therapy, or intralesional treatments (16).

Doxorubicin (DOX) is a therapeutic agent that has been studied in this context, although it is not approved for skin cancer. DOX's fluorescent properties allow it to function as a marker in drug delivery studies.

*_**Corresponding authors:**_ Fatemeh Ahmadi. Department of Pharmaceutics, School of Pharmacy, Shiraz University of Medical Sciences, Shiraz, Iran Email: ahmadi_f@sums.ac.ir; Shohreh Alipour. Department of Quality Control, School of Pharmacy, Shiraz University of Medical Sciences, Shiraz, Iran. Email: alipour_sh@sums.ac.ir

To minimize dose-limiting side effects of DOX, topical administration is preferred for skin cancer treatment. Studies suggest that topically administered DOX—either as polymeric conjugates or loaded into nanosized delivery systems—can maximize therapeutic efficacy against skin cancers, including melanoma (17-22). Several studies have evaluated the cytotoxicity of liposomal DOX on human metastatic melanoma, showing that it does not elicit a significant response in the metastatic form of the disease (23-25).

In the current study, the focus is on developing and evaluating hyaluronic acid (HA)-based polymeric micelles loaded with DOX. Polymeric micelles (PMs) are among the most promising systems for overcoming multidrug resistance and for targeting the tumor site (26). Hyaluronic acid-based polymeric micelles could act as a skin penetration enhancer with biodegradable and biocompatible properties (27).

Micelles will then be incorporated within the alginate-based hydrogel. Hydrogels are three-dimensional networks of cross-linked hydrophilic polymers. These structures are swollen by absorbing a large amount of water or biological fluids while maintaining their network structure. Hydrogels are advantageous for drug delivery to the skin due to their high water content and similar permeability and consistency to living tissues. Sodium alginate (SA) is one of the most commonly used natural polysaccharides, known for its unique gel-forming properties in the presence of multivalent cations in an aqueous environment. It is widely utilized as a gelling agent in the food industry. The gelation and cross-linking of alginate occur through the exchange of sodium ions with multivalent cations. Therefore, it is anticipated that embedding these micelles within alginate hydrogels, which provide a water-rich, tissue-mimicking network, can facilitate localized and controlled delivery of DOX to skin cancer tissues (28).

Although several studies have developed hybrid micelle–hydrogel platforms for DOX delivery to tumor cells (such as PLGA-PEG-PLGA micelles embedded in hyaluronic acid hydrogel). These systems have predominantly been designed as injectable in situ-forming systems rather than topical application. In many studies, the hydrogel component primarily served as a local depot to reduce burst release following intratumoral injection, while micelles enhanced intracellular uptake (29-31). However, limited attention has been given to adapting such hybrid architectures for transdermal chemotherapy, where prolonged surface residence, controlled diffusion across the stratum corneum, and minimized systemic exposure are critical. Moreover, most previously reported systems have focused on tumor models other than melanoma, despite the unique challenges associated with treating superficial skin malignancies (32-35). Therefore, the development of an HA-based micelle–hydrogel platform specifically tailored for topical melanoma therapy remains insufficiently explored. The present work aims to address this gap by investigating the potential of a topical hybrid delivery system—composed of oleic acid–modified hyaluronic acid micelles incorporated into a calcium alginate hydrogel—for localized, controlled delivery of DOX to skin cancer cells. Since DOX is not yet FDA-approved for use in skin cancer therapy, this work also aims to explore its potential as a candidate for this indication.

Materials and Methods

Materials

Hyaluronan (HA) (Mw = 15,000 g/mol) was purchased from Biosynth Ltd (United Kingdom). Oleic acid, Doxorubicin (DOX), 4-Dimethylaminopyridine (DMAP), 1-ethyl-(3-dimethylaminopropyl) carbodiimide hydrochloride (EDC), Dimethyl sulfoxide (DMSO), Acetonitrile (HPLC grade, 99.9%) were obtained from Merck (Germany). 3-(4,5-dimethyl-thiazol-2-yl)-2,5-diphenyl-tetrazolium bromide (MTT) was purchased from Sigma-Aldrich (USA). All reagents were of commercial grade. Deionized water (DIW) was used in all of the experiments of this study.

Synthesis and characterization of sodium oleyl hyaluronan

Hyaluronic Acid (0.5 g, 1.25 mmol) was dissolved in 10 ml of distilled water overnight. In another flask, oleic acid (0.39 ml, 1.25 mmol) was activated by EDC (0.15 ml, 1.25 mmol) and DMAP in DMSO (5 ml) (36). The formation of the active ester intermediate was performed overnight at room temperature. This solution was then added to the HA solution, and the reaction mixture was stirred for 12 hr at 25 °C. The reaction mixture was completely dialyzed against DIW/ethanol (70/30) and lyophilized to obtain HA-C18 copolymer.

The composition and structure of the copolymer were analyzed using a 300 MHz ^{1}H NMR spectrometer (Bruker AV-500, Germany).

Measurement of critical micelle concentration (CMC)

CMC of the HA-C18 polymer was determined using pyrene as a fluorescence probe (37). Initially, pyrene was dissolved in acetone, and the solvent was completely evaporated. Subsequently, HA–C18 aqueous solutions with concentrations ranging from 1.0×10^{-4} to 5.0×10^{-1} mg/ml were added to the pyrene residue. The resulting mixtures were sonicated for 30 min and then kept at room temperature in the dark overnight to allow equilibration prior to fluorescence measurement.

Fluorescence spectra were obtained using a fluorescence spectrometer (Bio-Tek Instruments Inc., USA). The excitation wavelength was set to 336 nm, and emission spectra were recorded from 360 nm to 450 nm. The CMC of HA–C18 was determined from the crossover point in the plot of the fluorescence intensity ratio of the third peak (I_3, 384 nm) to the first peak (I_1, 373 nm) versus the logarithm of polymer concentration (37).

Preparation of DOX-loaded HA-C18 micelles

DOX-loaded HA-C18 micelles were prepared by the film dispersion method (27). Briefly, the HA–C18 polymer and DOX (as base) were separately dissolved in DIW and chloroform, respectively. After mixing, the organic solvent was completely removed from the resulting mixture using a rotary vacuum evaporator at 40 °C to obtain a dry film. The film was subsequently dispersed in DIW, and the solution was centrifuged at 2500 rpm for 15 min to eliminate any unloaded DOX. Finally, the supernatant was collected and lyophilized to obtain the dried micellar product.

Optimization and characterization of DOX-loaded HA-C18 micelles

To optimize the preparation process, a D-optimal plan was generated using Design-Expert statistical software (version 13, Stat-Ease Inc., USA). The mass ratio of drug (DOX) to polymer and the ratio of organic phase to aqueous phase were two independent variables regarding the highest

loading of drug for 9 runs. The independent variables and dependent variable responses are listed in Table 1.

Particle size and size distribution

The average particle size and size distribution of DOX-loaded HA–C18 micelles were determined by dynamic light scattering (DLS) with a nanoparticle size analyzer (Horiba SZ-100, Japan). All measurements were conducted in triplicate at room temperature.

Transmission electron microscopy (TEM)

A drop of DOX-loaded HA–C18 micelle solution (0.5 mg/ml) was placed onto a copper grid and subsequently stained with a drop of 2% (w/v) phosphotungstic acid. The sample was then air-dried. The morphology of the DOX-loaded HA–C18 micelles was observed using a JEM-1400 transmission electron microscope (LEO, Germany) following standard procedures (36).

Assessment of drug entrapment efficiency (EE%) and drug loading (DL%)

To determine DOX content in the micelles, three milliliters of a DOX-loaded HA-C18 micellar solution were diluted with methanol, treated with ultrasonication for 3 min, and centrifuged at 5000 rpm for 5 min. DOX content was measured by UV spectrophotometry at 253 nm using a calibration curve (R^2 = 0.9989), with a limit of detection (LOD) and limit of quantification (LOQ) of 244.49 ± 0.002 ng/ml and 740.88 ± 0.002 ng/ml, respectively (38). Drug loading content (DL, wt%) and drug entrapment efficiency (EE, wt%) were calculated according to the following equations:

Equation 1: DL = (amount of loaded drug/amount of drug-loaded micelle) × 100%

Equation 2: EE = (amount of loaded drug / initial amount of drug added) × 100%

Preparation and characterization of micelle-loaded hydrogel

DOX-loaded HA-C18 micelles were added to a sodium alginate solution 1%, and the mixture was stirred overnight. Then, a 4% (w/v) calcium chloride solution was added dropwise to the hydrogel to cross-link it. pH of the hydrogel was determined in triplicate using a Sartorius PB-10 calibrated pH meter (Sartorius, Germany). Data are presented as mean ± standard deviation. The spreadability of the hydrogel was measured by the two-glass plate method. Half a gram of gel was placed on a glass slide, and a second glass slide weighing 42 g was positioned over it. The gel was allowed to spread under this load for 3 min, after which the diameter of the spread area was measured. The procedure was repeated with additional weights of 200 g and 500 g applied sequentially, each followed by a 3-min spreading period and measurement. The resulting spread areas were calculated and reported. All measurements were conducted in triplicate to guarantee accuracy and reproducibility (39). In addition, the storage stability of hydrogels was evaluated at 0, 1, and 3 months by determining the active pharmaceutical ingredient (API) content. Furthermore, the rheological characteristics of the hydrogel were studied using a Brookfield R/S Plus Rheometer (Brookfield Viscometer Ltd, Harlow, Essex, UK) fitted with a spindle and a Eurotherm cone/plate geometry to obtain viscosity and shear stress as a function of shear rate (40).

In vitro release study of micelle and hydrogel

The release behavior of DOX from HA-C18 micelle and hydrogel was evaluated using a membrane-less method in phosphate-buffered saline (PBS) at pH 7.4, with a pre-weighed empty glass tube (41). Tween 80 (0.5% w/v) was added to the solution to achieve sink conditions at 100 rpm and 37 °C. At determined time points (0.5, 2, 4, 8, 12, and 24 hr), samples were removed and centrifuged at 13,000 rpm for 15 min. The obtained supernatant was sonicated, and the amount of released DOX was determined by the validated UV spectrophotometric method (previously mentioned in 2.5.3). To investigate the release kinetics and elucidate the drug release mechanisms, DOX release data were fitted to various kinetic models, including zero-order, first-order, Higuchi, and Korsmeyer–Peppas equations. All measurements were performed in triplicate.

Ex vivo drug permeation study

The *ex vivo* permeation of the hydrogel was evaluated using excised rat skin in Franz diffusion cells under conditions simulating skin pH. Rats were euthanized by diethyl ether inhalation followed by cervical dislocation, and abdominal skin was collected (42). Hair was carefully removed without damaging the skin, which was then washed with PBS. The skin was mounted between the donor and receptor compartments of the diffusion cell, with the stratum corneum facing the donor compartment. The receptor compartment was filled with 36 ml of PBS (pH 7.5) with Tween 80 (0.5 % w/v), ensuring contact with the skin layer. The system was maintained at 37 ± 0.5 °C throughout the study, and the medium was stirred at 50 rpm. Different formulations were placed in the donor compartment, and 0.5 ml samples were withdrawn from the receptor compartment at predetermined time points (0, 0.5, 2, 4, 8, 12, and 24 hr). Fresh medium was immediately replaced to maintain a constant volume. Each sample was mixed with 0.5 ml of methanol, centrifuged, and the drug concentration was quantified using a validated HPLC method. The mobile phase consisted of DIW, methanol, and acetonitrile (50:10:40 v/v/v) at a flow rate of 1 ml/min. Detection was performed using a UV detector at 258 nm, with a runtime of 10 min, and the calibration curve (R^2 = 0.9983) showed an LOD of 178.91 ± 2.5 ng/ml and an LOQ of 542.16 ± 2.5 ng/ml.

In vitro cytotoxicity assay

The cytotoxicity of free DOX and DOX-loaded in micelle and unloaded micelle was tested by *in vitro* MTT assay (43). Briefly, B16-F10 melanoma cells were seeded into 96-well plates at a density of 5 × 10^3 cells per well and incubated for 24 hr at 37 °C for cell growth and attachment. Following this, the culture medium was removed and replaced with 200 µL of fresh medium containing various concentrations of the test samples. Cells were treated for 24 and 48 hr. To determine cell viability, 20 µL of MTT solution (5 mg/ml) was added to each well, and after incubation, cells were lysed using DMSO. The absorbance was measured using a microplate reader at 570 nm (test wavelength) and 630 nm (reference wavelength). Cell viability was expressed as a percentage relative to the untreated control group, which was set at 100% for each respective time point.

Flow cytometry analysis

The cellular uptake of micelles was investigated using

inverted fluorescence microscopy and flow cytometry (43). For the fluorescence microscopy experiments, B16-F10 cells were seeded into 6-well plates at a density of 1 × 10^5 cells per well and incubated overnight at 37 °C. Subsequently, the culture medium was replaced with serum-free medium containing either free DOX (DOX-Sol) or DOX-loaded micelles (DOX-PMs) (equivalent DOX concentration of 8 µg/ml), followed by 4 hr incubation at 37 °C. The cells were gently washed three times with cold PBS and fixed in 4% paraformaldehyde. After fixation, they were rinsed three times with cold PBS and incubated with Hoechst dye (100 ng/ml) for 10 min to stain the nuclei. Following a final triple wash with cold PBS, the cells were examined using a fluorescence microscope (Olympus CKX53, Japan).

For flow cytometric analysis, B16-F10 cells were seeded in 6-well plates at a density of 1 × 10^5 cells per well and cultured overnight at 37 °C. The cells were then incubated with either free DOX or DOX-PMs (equivalent DOX concentration of 8 µg/ml) for 4 hr at 37 °C. Subsequently, the cells were trypsinized, and the resulting cell suspensions were centrifuged at 1000 rpm for 3 min, washed twice with PBS, and resuspended in 0.5 ml of PBS. Fluorescence intensity was measured using a flow cytometer (Becton Dickinson, USA) with an excitation wavelength of 488 nm and an emission wavelength of 530 nm.

Results

Synthesis characterization of sodium oleyl hyaluronan

The HA–C18 conjugate was synthesized through a series of esterification reactions. The ^{1}H NMR spectra of HA and HA–C18 are presented in Figure 1. All observed signals could be assigned to either acyl or HA moieties:

Acyl signals: δ 0.9 (t, 3H, –CH_2–CH_3), 1.2–1.4 (m, 24H, (–CH_2–)$_{12}$), 1.6 (m, 2H, –CH_2–CH_2–CO–), 2.4 (t, 2H, –CH_2–CO–), 5.5 (m, 2H, CH=CH); HA signals: δ 2.0 (s, 3H, –NH–$COCH_3$), 3.1–3.9 (m, 10H, skeletal CH), 4.3–4.6 (m, 2H, anomeric CH).

The 1H NMR results confirmed the successful conjugation of the octadecyl group to the hyaluronic acid backbone, verifying the formation of the HA–C18 conjugate. Low–molecular–weight HA was used to prepare derivatives with a degree of substitution of 13.5%, resulting in products that were highly soluble in water and low-viscosity, facilitating their self-assembly into polymeric micelles in an aqueous environment.

CMC of the HA-C18 polymer

The CMC is a key parameter that governs the aggregation behavior of polymeric micelles in solution, thereby affecting the self-assembly properties of amphiphilic polymers and the structural stability of micelles in both *in vitro* and *in vivo* environments (36). The CMC of HA–C18 in aqueous solution was determined using fluorescence spectroscopy with pyrene as a hydrophobic probe. As shown in Figure 2, the fluorescence intensity ratio (I_3/I_1) was plotted against the logarithm of HA–C18 concentration, and the CMC was estimated from the threshold concentration at which micelle formation occurs. The HA–C18 polymer exhibited a low CMC value of 0.0625 mg/ml, markedly lower than that of conventional low-molecular-weight surfactants (44).

Optimization of the micelle preparation process

As mentioned, two independent variables, including the mass ratio of drug (DOX) to polymer and the ratio of

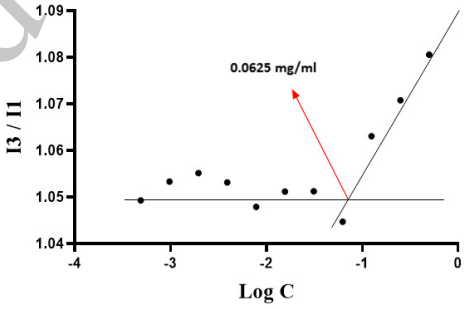

Figure 2. Plots of I3/I1 against logarithm of the HA-C18 concentration

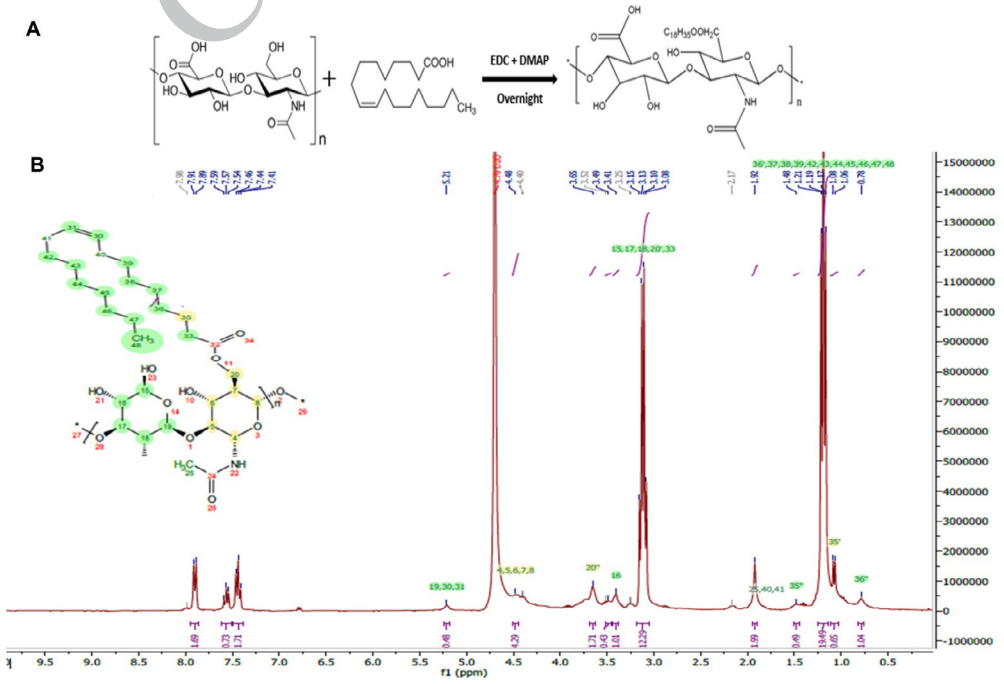

Figure 1. (A) Schematic representation of the synthesis of oleyl-hyaluronic acid (HA-C18) and 1H NMR spectrum of HA-C18 polymer

Table 1. Experimental design and results of the D-Optimal model responses

Run	Independent variables		Dependent variable	
	Dox/Polymer	Oil/Water	EE %	Particle size nm
1	0.1	0.5	30.6	226
2	0.2	0.5	37.3	410
3	0.05	0.167	10.1	216
4	0.2	0.167	39.1	399
5	0.05	0.5	10.8	220
6	0.1	0.167	24	230
7	0.2	0.25	40.1	399
8	0.05	0.25	11.3	219
9	0.1	0.25	28.7	230

organic phase to aqueous phase, along with the response of encapsulation efficiency (EE%) and particle size, were selected for the final optimization studies based on D-Optimal design. Table 1 demonstrates the results. ANOVA table for response surface quadratic model analysis of variance is also reported (Table 2). In the table, the *P*-value of the model < 0.05 indicates that the recommended model was significant for both responses. So, the presence of all of these factors was necessary to form an effective model; although *P*-values for the two factors indicate that the effects of the mass ratio of drug (DOX) to polymer on the developed model were significantly high. Based on achieving a smaller particle size and higher entrapment efficiency (EE%), the optimized formulation was established with a drug-to-polymer ratio of 1:10 and an organic-to-aqueous phase ratio of 0.25.

The particle size, size distribution, and zeta potential of the DOX-loaded HA-C18 micelles are shown in Figures 3A and 3B. The DOX-loaded HA-C18 micellar average size was approximately 221.4 ± 27 nm with a narrow size distribution. In addition, the particle size of DOX-loaded HA-C18 micelles was within a suitable range for accumulation in tumor tissue via the enhanced permeability and retention (EPR) effect (45). The DOX-PMs demonstrated relatively high stability, as evidenced by their zeta potential values of -44.3 ± 1.55 mV, an electrokinetic parameter commonly used to assess the stability of colloidal systems. TEM images of the DOX-loaded HA-C18 micelles are presented in Figure 3C, showing spherical micellar nanoaggregates with uniform size and core-shell structures. Moreover, the DOX-loaded HA-C18 micelles demonstrated a drug loading efficiency of about 4.32 ± 0.5 %, likely resulting from the strong hydrophobic interactions and tight entrapment of DOX within the micellar core.

Preparation and characterization of micelle-loaded hydrogel

In melanoma, the microenvironment of the cancerous tissue is typically acidic, with a pH lower than that of normal

Table 2. ANOVA results of D-optimal model developed for design of the experiment

Source		Sum of squares	df	Mean square	F-value	*P*-value	
Response 1: EE %	Model	1215.47	6	202.58	27.77	0.0352	Significant
	A-DOX/Polymer	1088.86	1	1088.86	149.26	0.0066	
	B-Oil/Water	8.97	2	4.43	0.6079	0.6219	
Response 2: particle size	Model	64422.94	6	10737.16	556.05	0.0018	Significant
	A-DOX/Polymer	59323.46	1	59323.46	3072.24	0.0003	
	B-Oil/Water	21.56	2	10.78	0.5582	0.6418	

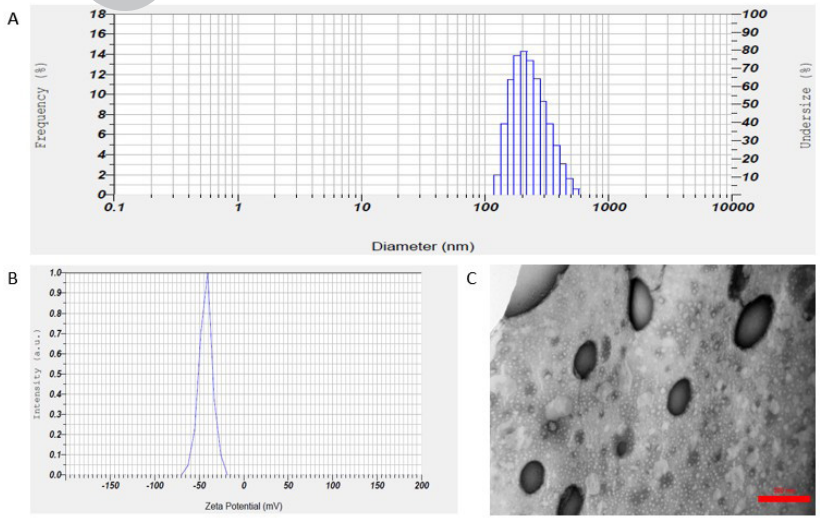

Figure 3. (A) Particle size, (B) zeta potential, and (C) TEM image of the micelles

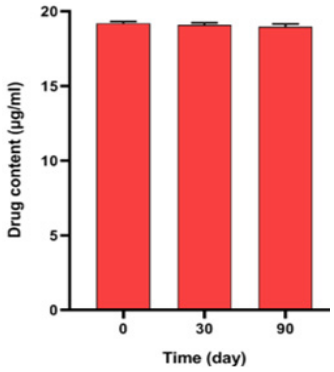

Figure 4. Assessment of the stability of drug content throughout the storage period at room temperature

skin, due to the metabolic activity of melanoma cells. The pH of the hydrogel was 4.51 ± 0.02, corresponding to the physiological pH of melanoma. Furthermore, uniform skin distribution of the product relies on its spreadability. Improved spreadability facilitates patient compliance and ensures consistent application. The hydrogel exhibited spreading areas of 13.63 ± 0.24 cm^2 (diameter 4.1 cm), 23.19 ± 0.094 cm^2 (diameter 5.43 cm), and 37.75 ± 0.094 cm^2 (diameter 6.93 cm) after placing the 42g glass plate and applying 200 g and 500 g weights, respectively. These results indicated a favorable spreading behavior of the hydrogel. As shown in Figure 4, stability assessment of the hydrogel at room temperature (25 °C) revealed that the drug content was almost unchanged within 90 days without significant reduction (less than 3%) and drug expulsion. In addition, viscosity and shear stress were plotted against shear rate for the prepared hydrogel. The sample exhibited a decrease in viscosity and an increase in shear stress as the shear rate increased (Figure 5). The slope of the shear stress versus shear rate curve (apparent viscosity) rises sharply as the shear rate decreases, confirming the shear-thinning behavior of alginate-based hydrogel, as presented by viscosity measurements; the alginate formulation exhibited a viscosity of 3.2 Pa. (46).

Drug release and kinetic studies

The drug release behavior of DOX-loaded HA-C18 micelles and hydrogel was investigated through a membrane-less method in PBS (pH 7.5) containing 1% Tween 80 at 37 °C. As shown in Figure 6, the DOX-loaded HA-C18 micelles released 60% of DOX within 24 hr, while the hydrogel released 40% of DOX during 24 hr. The micelle and hydrogel exhibited burst release at 0.5 hr, followed by prolonged release for up to 24 hr.

The initial burst release observed in the release profile may be ascribed to the low molecular weight of the polymer, especially the hydrophobic domain, which compromises the structural stability of the micellar cores and facilitates rapid diffusion of DOX (47).

To evaluate the kinetics of DOX release from the micelle and hydrogel, the release data from 0.5 to 24 hr were fitted to zero-order, first-order, Higuchi, and Korsmeyer-Peppas kinetic models. The model with both the highest R^2 and the lowest percent error (E%) was recommended as the best-fit model. Based on the data in Table 3, the Higuchi model best fits the micelle, meeting the specified criterion. Drug release from the micelle is primarily via Fickian diffusion (n=0.08). However, the drug release of the hydrogel is

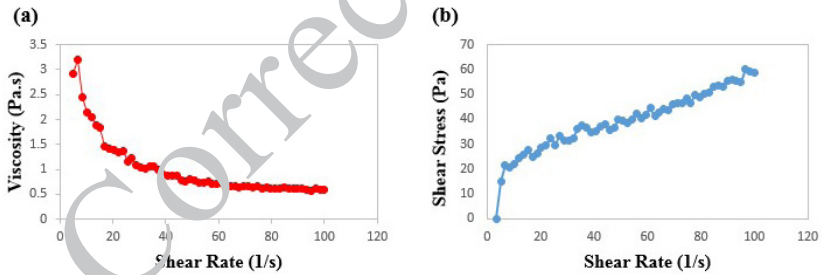

Figure 5. (a) Viscosity and (b) shear stress as a function of shear rate for the hydrogel at 25 °C

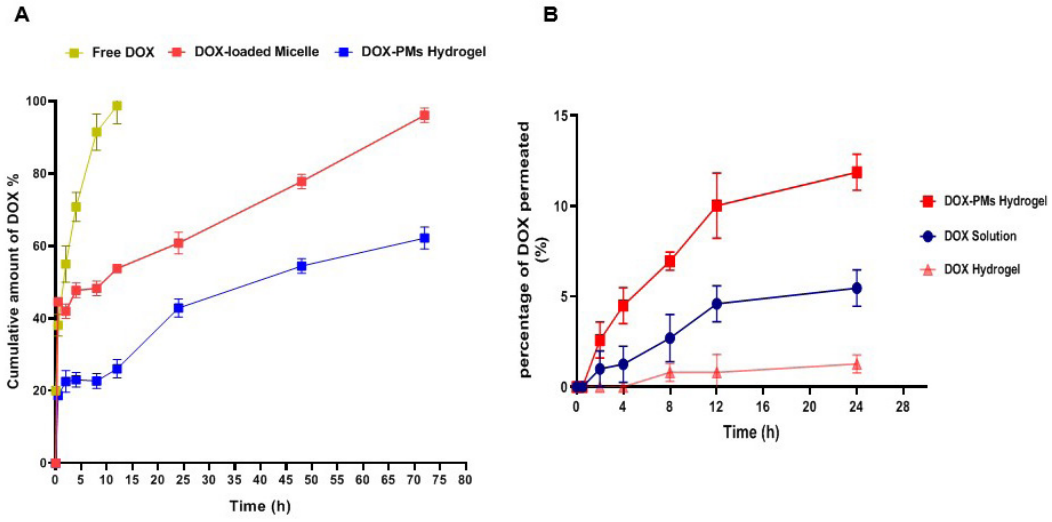

Figure 6. Release profile (A) and *ex vivo* permeation profile (B) of DOX

Table 3. Results of evaluating release kinetics by curve fitting model

Model		R^2	E%
Micelle	Zero order	0.9291	- 8.5
	First order	0.947	-8.37
	Higuchi	0.9461	-8.31
	Korsmeyer-Peppas	0.7191	-9.21
Hydrogel	Zero order	0.9191	83.32
	First order	0.9009	83.61
	Higuchi	0.8833	83.74
	Korsmeyer-Peppas	0.6782	81.51

based on anomalous transport (n=0.67), and release data demonstrated a better fit with zero-order and Hixson-Crowell models. Data are presented in Table 3. Therefore, the release mechanism is controlled by surface erosion and structural degradation, not just by diffusion.

Ex vivo drug permeation result

Ex vivo permeation profile of DOX solution, DOX-loaded hydrogel, and DOX-PMs-hydrogel (DOX-loaded micelle in hydrogel) was determined through a Franz cell in the same medium and conditions as the *in vitro* release study (Figure 6.B). The results of this study showed that HA-C18 micelles were able to markedly enhance the transdermal permeation of DOX. In the Franz diffusion assay, the micelle-containing formulation transferred considerably higher drug across the skin compared with both the free DOX solution and the DOX-loaded alginate hydrogel. After 24 hr, the micellar formulation achieved approximately a 2.1-fold increase in permeation relative to the free drug solution and a 9.2-fold increase compared with the plain alginate hydrogel. These findings clearly indicate that the micellar structure itself is responsible for the improved skin penetration of DOX. In addition, the alginate matrix, placed at the final stage of formulation, primarily functioned as a release-modulating scaffold.

In vitro cytotoxicity assay

The cytotoxicity of free DOX and DOX-loaded micelle and unloaded micelle was tested by *in vitro* MTT assay. According to Figure 7, both free DOX and DOX-PMs significantly reduced the viability of B16F10 cells as drug concentration and incubation time increased. IC_{50} values of DOX-PMs after 24-hr and 48-hr treatment were 12.9 µg/ml and 4.6 µg/ml, respectively. Compared to free DOX, DOX-PMs demonstrated lower cytotoxicity at equivalent DOX concentration. As a small molecule, free DOX rapidly diffused into cells and subsequently reached its active site within the nucleus through passive diffusion. In contrast, DOX-PMs were internalized by cells exclusively via endocytosis, and only the DOX released from the micelles could penetrate the nucleus. Therefore, it can be concluded that with an increase in the concentration of DOX in the micelle, cytotoxicity was enhanced. For instance, at higher concentrations, such as 20 µg/ml, and with a longer incubation time, specifically a 48-hr period, there was a slight increase in cytotoxicity compared to the free DOX. This might be explained as well by the slower release of DOX from the micelle, previously shown in Figure 5. Overall, during the 48-hr incubation period, cytotoxicity was significantly higher than during the 24-hr period, indicating accumulation of DOX in the cells and increased toxicity.

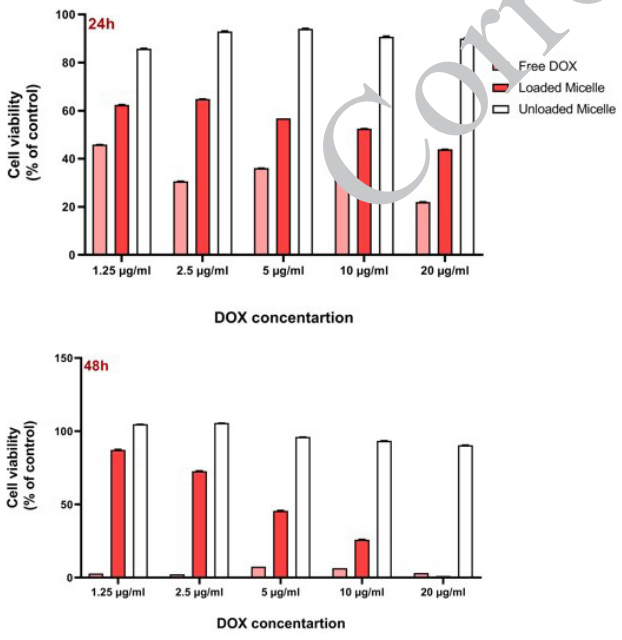

Figure 7. Viability of B16F10 cells as a function of DOX concentration (1.25, 2.5, 5, 10, and 20 µg/ml) and incubation time (24 and 48 hr)
DOX: Doxorubicin

Flow cytometry analysis

Cellular uptake of DOX formulations was evaluated in B16F10 cells by flow cytometry and fluorescence microscopy.

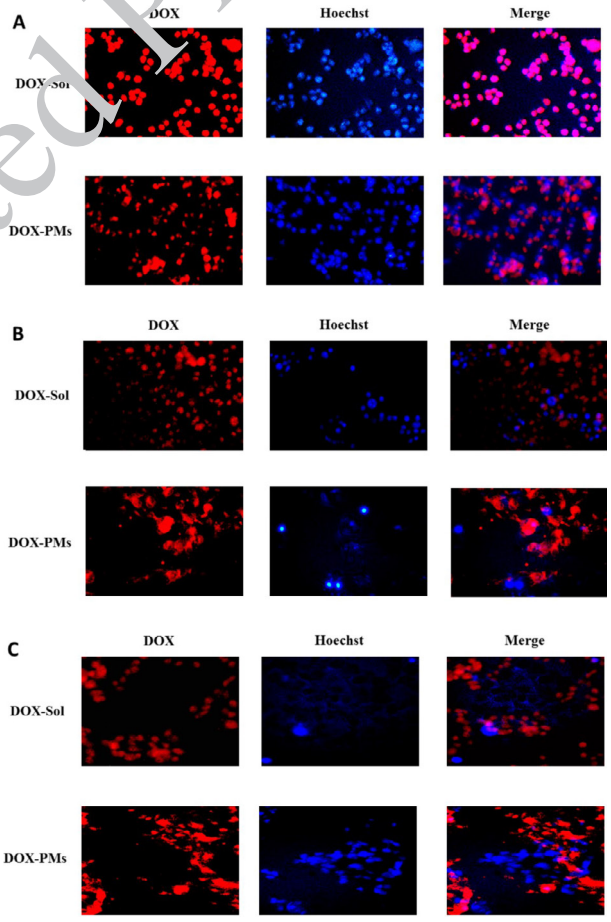

Figure 8. Fluorescence microscopy images of DOX solution (DOX-Sol), Dox micelles (DOX-PMs) after incubation with 1 h (A), 2 h (B) and 4 h (C) in B16F10 cells
Cells were counterstained with Hoechst for nuclei
DOX: Doxorubicin; DOX-PMs: DOX-loaded micelles

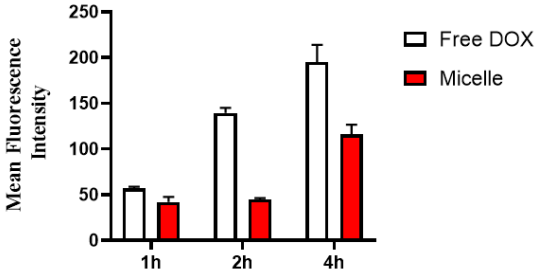

Figure 9. Flow cytometry analysis of cellular uptake of DOX in B16F10 cells after incubation with Free DOX and DOX micelles, for 1 hr, 2 hr, and 4 hr, respectively
DOX: Doxorubicin

According to the fluorescent microscopy images (Figure 8), cellular uptake of DOX at 1, 2, and 4-hr time intervals was observed for both free DOX (DOX-Sol) and DOX-loaded micelles (DOX-PMs) at an equal concentration of 8 µg. In all images, cellular uptake was evident, indicating that the micelles were able to deliver DOX into the cells. With increasing incubation time, cell death increased, consistent with previously reported studies. However, quantitative analysis, reported as mean fluorescence intensity, reveals a noticeable difference (Figure 9). Obviously, DOX was released from the micelles gradually, which consequently suggests that the rate of cellular uptake of DOX was expected to be lower than that of free DOX. This means that cellular uptake of DOX in all formulations was time-dependent. However, decreasing this difference over time indicates a slower release of DOX from the micelles. As shown in Figure 9, there is no significant difference in the average fluorescence intensity between free DOX and DOX-loaded micelles at the 1-hr interval. At the 2-hr interval, this difference was significant, indicating the rapid uptake and accumulation of free DOX. However, at the 4-hr interval, the DOX released from the micelles showed a much higher accumulation than at the 2-hr interval, again highlighting the slow release of DOX from the micelles.

Discussion

Localized chemotherapy for skin cancer remains clinically challenging due to the intrinsic barrier function of the stratum corneum, which leads to sub-therapeutic concentration of the drug at the site. Nanocarrier-based topical systems have been proposed to overcome these limitations; however, many platforms suffer from insufficient skin retention, burst release, or structural instability. In this context, the present study introduces a rationally designed hybrid system that integrates oleic acid–modified hyaluronic acid (HA-C18) micelles into an alginate hydrogel matrix to synergistically enhance dermal penetration, drug retention, and controlled release. The hybrid system improves DOX delivery through complementary mechanisms at both the nanoscale and macroscopic levels. The HA-C18 micelles enhance drug solubility and facilitate penetration across the stratum corneum due to their amphiphilic structure and nanoscale size. The predominant penetration pathway of the HA vehicle is transcellular (27). Simultaneously, the alginate hydrogel increases skin retention time and provides sustained release, ensuring prolonged drug availability at the application site. The combined effect results in enhanced transdermal transport, increased local drug concentration within superficial melanoma tissues, and reduced systemic exposure compared to free DOX.

Chemical modification of hyaluronic acid with oleic acid successfully generated an amphiphilic polymer capable of self-assembly into stable nano-sized micelles. Modified polysaccharides can form micelles in water through various techniques such as film dispersion, dialysis, ultrasonication, or emulsification, depending on their solubility and swelling behavior. In this study, DOX-loaded HA–C18 micelles were prepared using the film dispersion method. The polymer and drug were dissolved in aqueous and organic solvents, respectively, followed by solvent removal under reduced pressure. A dry film was formed and then hydrated to generate micelles. Self-assembly was driven by hydrophobic interactions among the grafted octadecyl chains forming the micellar core, and the hydrophilic HA backbone formed the shell, providing steric stabilization. The nanoscale dimension and relatively narrow size distribution indicate efficient self-organization and colloidal stability, which are critical parameters for enhancing skin penetration and intracellular uptake. Effective dermal delivery requires the active compounds to permeate into deeper skin layers, particularly the dermis, where they exert their effects. Enhancing transdermal transport of hydrophobic molecules is crucial for improving their cutaneous bioavailability. Previous studies have shown that low-molecular-weight hyaluronic acid can promote the penetration of both small and large hydrophilic molecules into the skin (27, 48, 49). The hydrophobic core of HA-C18 micelles provided an efficient reservoir for DOX encapsulation, improving drug solubility and protecting it from premature degradation. Additionally, a low CMC value suggests that desirable structural integrity can be achieved even at low polymer concentration, and that the micelles exhibit higher structural stability both *in vitro* and *in vivo* (44). In aqueous media, the zeta potential ranged from approximately –40 to –70 mV, depending on the concentration of the polymeric micelles. These relatively high absolute zeta potential values indicate excellent to very good stability of HA polymeric micelles in aqueous solutions (50). Hence, the negative zeta potential of the polymeric micelles (-44.3 ± 1.55 mV), originating from the dissociated carboxyl groups of HA, was theoretically expected to induce electrostatic repulsion with the negatively charged stratum corneum and cell membranes and thereby promote transport of the drug (27, 51). Furthermore, an appropriate DL% of the polymeric micelle is very important for DOX-loaded HA-C18 micelle, especially when it is designed for transdermal delivery.

While polymeric micelles alone can enhance permeation, they often diffuse rapidly away from the application site when used topically. Embedding DOX-PMs within an alginate hydrogel addressed this limitation by introducing a secondary diffusion barrier and a structural depot effect. Similar hybrid micelle–hydrogel systems reported in the literature have shown improved local retention in injectable or in situ–forming platforms; however, most have focused on subcutaneous or intratumoral administration rather than transdermal chemotherapy (32-35). In contrast, the present study specifically targets topical melanoma therapy, where prolonged residence time and controlled release are critical for therapeutic efficacy. Accordingly, the alginate hydrogel (3.2 Pa·s at 1 s^{-1}) exhibited shear-thinning behavior, enabling easy spreading during application while maintaining structural stability and extended retention at the skin surface (52).

The release profile observed in this study reflects the

cooperative diffusion provided by both the micellar core and the alginate hydrogel network. Additionally, kinetic studies of drug release from carriers are helpful for identifying the key factors influencing release rates and for optimizing conditions to achieve the desired *in vivo* release profile (53, 54). Consistent with previous reports on HA-based amphiphilic micelles, which demonstrated markedly enhanced intradermal deposition of hydrophobic agents compared with non-micellar systems, our findings confirm the critical role of micellar architecture in promoting skin penetration (27). Specifically, the incorporation of HA-C18 micelles resulted in an approximately 2.1-fold increase in 24-hour permeation compared with free DOX and a 9.2-fold increase relative to alginate hydrogel without micelles, highlighting the micelles as the primary driver of enhanced transport. While the alginate matrix did not significantly improve permeation, it functioned effectively as a release-modulating depot, ensuring prolonged surface retention and potentially limiting systemic exposure (29, 55). DOX has been reported to exhibit similar release profiles in micellar and micelle–hydrogel hybrid systems, where release kinetics are mainly governed by diffusion from the micellar core rate (29). However, in the present study, drug release was predominantly controlled by hydrogel matrix erosion and geometric structural changes, resulting in a nearly constant release rate (56). By balancing enhanced penetration with controlled retention, this hybrid platform also reduces the likelihood of DOX entering the bloodstream in clinically significant amounts while preserving the micelle's ability to facilitate drug penetration into the targeted superficial layers.

The *in vitro* cytotoxicity results showed lower IC_{50} values for free DOX than DOX-PMs, reflecting its rapid passive diffusion into cells and immediate nuclear accumulation (50, 57-59). In contrast, micellar DOX required endocytic uptake and subsequent intracellular release, leading to a slower onset of cytotoxicity. However, both cytotoxicity and flow cytometry analyses demonstrated a time-dependent increase in intracellular accumulation for the micellar formulation, indicating sustained drug release and progressive cellular uptake. These findings suggest that micellar encapsulation modifies the delivery kinetics of DOX, providing prolonged intracellular exposure that may be advantageous for controlled and localized melanoma therapy.

Collectively, this study advances the field of localized chemotherapy by demonstrating that the strategic integration of amphiphilic HA-based micelles with a biocompatible hydrogel matrix can simultaneously overcome multiple barriers—penetration, retention, and release control. By bridging nanotechnology and biomaterial engineering, the HA-C18 micelle–alginate hydrogel platform represents a rational and potentially translatable approach to improving the therapeutic index of DOX in the management of superficial melanoma.

Conclusion

This study introduces a novel topical delivery platform that combines oleic acid–modified hyaluronic acid (HA-C18) micelles with an alginate hydrogel for DOX administration. The micelles function as potent penetration enhancers, while the hydrogel provides sustained release and prolonged skin retention, together enabling superior transdermal transport compared with free drug or hydrogel alone. This hybrid design offers significant therapeutic potential for superficial skin cancer, enabling localized, controlled drug delivery with minimized systemic exposure and providing a translationally relevant, patient-compatible strategy for localized chemotherapy. Future studies focusing on *in vivo* performance and receptor-mediated uptake will be critical to fully validate and optimize this platform for clinical application.

Acknowledgment

This study was part of the PhD thesis of Majid Zia-Behbahani and was funded by Shiraz University of Medical Sciences, Shiraz, Iran (Grant No. 24309).

Authors' Contributions

M ZB handled project administration, methodology, and formal analysis, and drafted the original manuscript. E P contributed through supervision, methodology, formal analysis, data curation, original drafting, visualization, and review/editing. MH A was responsible for project administration, methodology, and formal analysis. E E provided supervision, project management, methodology, and oversight. S A supervised and managed the project, contributed to methodology, performed formal analysis, curated data, and reviewed and edited. F A supervised and managed the project, contributed to methodology, performed formal analysis, curated data, created visualizations, and reviewed and edited.

Conflicts of Interest

The authors declare no conflicts of interest.

Declaration

We acknowledge the use of ChatGPT version 5.3-mini for linguistic refinement of the Introduction section of the manuscript.

References

1. Mayo clinic. Skin cancer 2020 [cited 2020]. Available from: https://www.mayoclinic.org/diseases-conditions/skin-cancer/symptoms-causes/syc-20377605.
2. Apalla Z, Lallas A, Sotiriou E, Lazaridou E, Ioannides D. Epidemiological trends in skin cancer. Dermatol Pract Concept 2017; 7:1-6.
3. Mattia G, Puglisi R, Ascione B, Malorni W, Carè A, Matarrese P. Cell death-based treatments of melanoma: Conventional treatments and new therapeutic strategies. Cell Death Dis 2018; 9:112.
4. Domingues B, Lopes JM, Soares P, Pópulo H. Melanoma treatment in review. Immunotargets Ther 2018; 7:35-49.
5. Schadendorf D, van Akkooi AC, Berking C, Griewank KG, Gutzmer R, Hauschild A, *et al.* Melanoma. Lancet 2018; 392:971–984.
6. Gandini S, Autier P, Boniol M. Reviews on sun exposure and artificial light and melanoma. Prog Biophys Mol Biol 2011; 107:362–366.
7. Boniol M, Autier P, Boyle P, Gandini S. Cutaneous melanoma attributable to sunbed use: Systematic review and meta-analysis. BMJ 2012; 345.
8. Berwick M, Erdei E, Hay J. Melanoma epidemiology and public health. Dermatol Clin 2009; 27:205–214.
9. Flohil SC, van der Leest RJ, Arends LR, de Vries E, Nijsten T. Risk of subsequent cutaneous malignancy in patients with prior keratinocyte carcinoma: A systematic review and meta-analysis. Eur J Cancer 2013; 49:2365–2375.
10. Eide MJ, Krajenta R, Johnson D, Long JJ, Jacobsen G, Asgari MM, *et al.* Identification of patients with nonmelanoma skin cancer using health maintenance organization claims data. Am J

Epidemiol 2010; 171:123–128.
11. Wadhera A, Fazio M, Bricca G, Stanton O. Metastatic basal cell carcinoma: A case report and literature review. How accurate is our incidence data? Dermatol Online J 2006; 12:7.
12. Dummer R, Hauschild A, Lindenblatt N, Pentheroudakis G, Keilholz U. Cutaneous melanoma: ESMO clinical practice guidelines for diagnosis, treatment and follow-up. Ann Oncol 2015; 26:v126–v132.
13. Li J, Wang Y, Liang R, An X, Wang K, Shen G, *et al.* Recent advances in targeted nanoparticles drug delivery to melanoma. Nanomedicine 2015; 11:769–794.
14. Rapozzi V, Jori G. Resistance to photodynamic therapy in cancer: Springer; 2014.
15. Widakowich C, de Castro Jr G, De Azambuja E, Dinh P, Awada A. Side effects of approved molecular targeted therapies in solid cancers. Oncologist 2007; 12:1443–1455.
16. Austin E, Mamalis A, Ho D, Jagdeo J. Laser and light-based therapy for cutaneous and soft-tissue metastases of malignant melanoma: A systematic review. Arch Dermatol Res 2017; 309:229–242.
17. Krishnan V, Peng K, Sarode A, Prakash S, Zhao Z, Filippov SK, *et al.* Hyaluronic acid conjugates for topical treatment of skin cancer lesions. Sci Adv 2021; 7:eabe6627.
18. Lv Q, He C, Quan F, Yu S, Chen X. DOX/IL-2/IFN-γ co-loaded thermo-sensitive polypeptide hydrogel for efficient melanoma treatment. Bioact Mater 2018; 3:118–128.
19. Tupal A, Sabzichi M, Ramezani F, Kouhsoltani M, Hamishehkar H. Dermal delivery of doxorubicin-loaded solid lipid nanoparticles for the treatment of skin cancer. J Microencapsul 2016; 33:372–380.
20. Ahmed KS, Shan X, Mao J, Qiu L, Chen J. Derma roller® microneedles-mediated transdermal delivery of doxorubicin and celecoxib co-loaded liposomes for enhancing the anticancer effect. Mater Sci Eng C Mater Biol Appl 2019; 99:1448–1458.
21. Huber LA, Pereira TA, Ramos DN, Rezende LC, Emery FS, Sobral LM, *et al.* Topical skin cancer therapy using doxorubicin loaded cationic lipid nanoparticles and iontophoresis. J Biomed Nanotechnol 2015; 11:1975–1988.
22. Wang W, Zhang P, Shan W, Gao J, Liang W. A novel chitosan-based thermosensitive hydrogel containing doxorubicin liposomes for topical cancer therapy. J Biomater Sci Polym Ed 2013; 24:1649–1659.
23. Smylie MG, Wong R, Mihalcioiu C, Lee C, Poulliot JF. A phase II, open label, monotherapy study of liposomal doxorubicin in patients with metastatic malignant melanoma. Invest New Drugs 2007; 25:155–159.
24. Ugurel M, Schadendorf D, Fink W, Zimpfer-Rechner C, Thoelke A, Figl R, *et al.* Clinical phase II study of pegylated liposomal doxorubicin as second-line treatment in disseminated melanoma. Onkologie 2004; 27:540–544.
25. Vorobiof DA, Rapoport BL, Mahomed R, Karime M. Phase II study of pegylated liposomal doxorubicin in patients with metastatic malignant melanoma failing standard chemotherapy treatment. Melanoma Res 2003; 13:201–203.
26. Wang J, Li Y, Wang L, Wang X, Tu P. Comparison of hyaluronic acid-based micelles and polyethylene glycol-based micelles on reversal of multidrug resistance and enhanced anticancer efficacy *in vitro* and *in vivo*. Drug Deliv 2018; 25:330–340.
27. Šmejkalová D, Muthný T, Nešporová K, Hermannová M, Achbergerová E, Huerta-Angeles G, *et al.* Hyaluronan polymeric micelles for topical drug delivery. Carbohydr Polym 2017; 156:86–96.
28. Abasalizadeh F, Moghaddam SV, Alizadeh E, akbari E, Kashani E, Fazljou SMB, *et al.* Alginate-based hydrogels as drug delivery vehicles in cancer treatment and their applications in wound dressing and 3D bioprinting. J Biol Eng 2020; 14:8.
29. Wei L, Cai C, Lin J, Chen T. Dual-drug delivery system based on hydrogel/micelle composites. Biomaterials 2009; 30:2606–2613.
30. Zang C, Tian Y, Tang Y, Tang M, Yang D, Chen F, *et al.* Hydrogel-based platforms for site-specific doxorubicin release in cancer therapy. J Transl Med 2024; 22:879.
31. Rakhshani N, Hassanzadeh Nemati N, Saadatabadi AR, Sadrnezhaad SK. Fabrication of novel poly(N-vinylcaprolactam)-coated UiO-66-NH2 metal organic framework nanocarrier for the controlled release of doxorubicin against A549 lung cancer cells. J Drug Del Sci Tech 2021; 66:102881.
32. Li W, Tao C, Wang J, Le Y, Zhang J. MMP-responsive in situ forming hydrogel loaded with doxorubicin-encapsulated biodegradable micelles for local chemotherapy of oral squamous cell carcinoma. RSC Adv 2019; 9:31264–31273.
33. Liu M, Song X, Wen Y, Zhu J-L, Li J. Injectable thermoresponsive hydrogel formed by alginate-g-poly(N-isopropylacrylamide) that releases doxorubicin-encapsulated micelles as a smart drug delivery system. ACS Appl Mater Interfaces 2017; 9:35673–35682.
34. Domiński A, Konieczny T, Godzierz M, Musioł M, Janeczek H, Foryś A, *et al.* Co-delivery of 8-Hydroxyquinoline glycoconjugates and doxorubicin by supramolecular hydrogel based on α-Cyclodextrin and pH-responsive micelles for enhanced tumor treatment. Pharmaceutics 2022; 14:2490.
35. Chung CK, García-Co... Campos Y, Kralisch D, Bierau K, Chan A, *et al.* Doxorubicin loaded poloxamer thermosensitive hydrogels: Chemical, pharmacological and biological evaluation. Molecules 2020; 25:2219.
36. Xi Y, Jiang T, Yu Y, Yu J, Xue M, Xu N, *et al.* Dual targeting curcumin loaded alendronate-hyaluronan- octadecanoic acid micelles for improving osteosarcoma therapy. Int J Nanomed 2019; 14:6425–6437.
37. Niu L, Yuan M, Zhang Z, Wang L, Fan Y, Liu X, *et al.* Hyaluronic acid micelles for promoting the skin permeation and deposition of curcumin. Int J Nanomed 2022; 17:4009–4022.
38. Lv S, Wu Y, Cai K, He H, Li Y, Lan M, *et al.* High drug loading and sub-quantitative loading efficiency of polymeric micelles driven by donor–receptor coordination interactions. J Am Chem Soc 2018; 140:1235–1238.
39. Szulc-Musioł B, Siemiradzka W, Dolińska B. Formulation and evaluation of hydrogels based on sodium alginate and cellulose derivatives with quercetin for topical application. Applied Sci 2023; 13:7826.
40. Xu M, Mou Y, Hu M, Dong W, Su X, Wu R, *et al.* Evaluation of micelles incorporated into thermosensitive hydrogels for intratumoral delivery and controlled release of docetaxel: A dual approach for *in situ* treatment of tumors. Asian J Pharm Sci 2018; 13:373–382.
41. Nie S, Hsiao WW, Pan W, Yang Z. Thermoreversible Pluronic® F127-based hydrogel containing liposomes for the controlled delivery of paclitaxel: *in vitro* drug release, cell cytotoxicity, and uptake studies. Int J Nanomedicine 2011:151–166.
42. Kumari S, Alsaidan OA, Mohanty D, Zafar A, Das S, Gupta JK, *et al.* Development of soft luliconazole invasomes gel for effective transdermal delivery: Optimization to *in-vivo* antifungal activity. Gels 2023; 9:626.
43. Ma W, Guo Q, Li Y, Wang X, Wang J, Tu P. Co-assembly of doxorubicin and curcumin targeted micelles for synergistic delivery and improving anti-tumor efficacy. Eur J Pharm Biopharm 2017; 112:209–223.
44. Cho HJ, Yoon HY, Koo H, Ko SH, Shim JS, Lee JH, *et al.* Self-assembled nanoparticles based on hyaluronic acid-ceramide (HA-CE) and Pluronic® for tumor-targeted delivery of docetaxel. Biomaterials 2011; 32:7181–7190.
45. Iyer AK, Khaled G, Fang J, Maeda H. Exploiting the enhanced permeability and retention effect for tumor targeting. Drug Discov Today 2006; 11:812–818.
46. Cuomo F, Cofelice M, Lopez F. Rheological characterization of hydrogels from alginate-based nanodispersion. Polymers (Basel) 2019; 11:259.

47. Cui C, Xue YN, Wu M, Zhang Y, Yu P, Liu L, *et al.* Cellular uptake, intracellular trafficking, and antitumor efficacy of doxorubicin-loaded reduction-sensitive micelles. Biomaterials 2013; 34:3858–3869.
48. Williams AC, Barry BW. Penetration enhancers. Adv Drug Deliv Rev 2004; 56:603–618.
49. Witting M, Boreham A, Brodwolf R, Vávrová K, Alexiev U, Friess W, *et al.* Interactions of hyaluronic acid with the skin and implications for the dermal delivery of biomacromolecules. Mol Pharm 2015; 12:1391–1401.
50. Smejkalová D, Nešporová K, Hermannová M, Huerta-Angeles G, Cožíková D, Vištejnová L, *et al.* Paclitaxel isomerisation in polymeric micelles based on hydrophobized hyaluronic acid. Int J Pharm 2014; 466:147–155.
51. Yang Y, Sunoqrot S, Stowell C, Ji J, Lee C-W, Kim JW, *et al.* Effect of size, surface charge, and hydrophobicity of poly(amidoamine) dendrimers on their skin penetration. Biomacromolecules 2012; 13:2154–2162.
52. Cao H, Wang M, Ding J, Lin Y. Hydrogels: A promising therapeutic platform for inflammatory skin diseases treatment. J Mater Chem B 2024; 12:8007–8032.
53. Barati M, Mohammadi Samani S, Pourtalebi Jahromi L, Ashrafi H, Azadi A. Controlled-release in-situ gel forming formulation of tramadol containing chitosan-based pro-nanogels. Int J Biol Macromol 2018; 118:1449–1454.
54. Azadi A, Hamidi M, Rouini M-R. Methotrexate-loaded chitosan nanogels as 'Trojan Horses' for drug delivery to brain: Preparation and in vitro/*in vivo* characterization. Int J Biol Macromol 2013; 62:523–530.
55. Zang C, Tian Y, Tang Y, Tang M, Yang D, Chen F, *et al.* Hydrogel-based platforms for site-specific doxorubicin release in cancer therapy. J Transl Med 2024; 22:879.
56. Gill KK, Nazzal S, Kaddoumi A. Paclitaxel loaded PEG5000–DSPE micelles as pulmonary delivery platform: Formulation characterization, tissue distribution, plasma pharmacokinetics, and toxicological evaluation. Eur J Pharm Biopharm 2011; 79:276–284.
57. Alipour S, Shirazi HC, Kazemi M, Dehshahri A, Ahmadi F. Synthesis and cytotoxicity evaluation of doxorubicin-polyethyleneimine conjugate as a potential carrier for dual delivery of drug and gene. J Drug Deliv Sci Technol 2022; 68:102994.
58. Mansouri K, Ahmadi F, Dehshahri A. Synthesis of L-DOPA conjugated doxorubicin-polyethyleneimine nanocarrier and evaluation of its cytotoxicity on A375 and HepG2 cell lines. Nanomed J 2021; 8:264-269.
59. Kazemi M, Parhizkar E, Samani SM, Firuzi O, Sadeghpour H, Ahmadi F, *et al.* Targeted co-delivery of paclitaxel and anti P-gp shRNA by low molecular weight PEI decorated with L-3, 4-dihydroxyphenylalanine. Biotechnol Prog 2023; 39:e3310.